

Active Suppression of Interneuron Programs within Developing Motor Neurons Revealed by Analysis of Homeodomain Factor HB9

Joshua Thaler,* Kathleen Harrison,† Kamal Sharma,* Karen Lettieri,* John Kehrl,† and Samuel L. Pfaff*†

*Gene Expression Laboratory
The Salk Institute for Biological Studies
La Jolla, California 92037

†Laboratory of Immunoregulation
National Institute of Allergy
and Infectious Diseases
National Institutes of Health
Bethesda, Maryland 20892

Summary

Sonic hedgehog (Shh) specifies the identity of both motor neurons (MNs) and interneurons with morphogen-like activity. Here, we present evidence that the homeodomain factor HB9 is critical for distinguishing MN and interneuron identity in the mouse. Presumptive MN progenitors and postmitotic MNs express HB9, whereas interneurons never express this factor. This pattern resembles a composite of the avian homologs MNR2 and HB9. In mice lacking *Hb9*, the genetic profile of MNs is significantly altered, particularly by upregulation of *Chx10*, a gene normally restricted to a class of ventral interneurons. This aberrant gene expression is accompanied by topological disorganization of motor columns, loss of the phrenic and abducent nerves, and intercostal nerve pathfinding defects. Thus, MNs actively suppress interneuron genetic programs to establish their identity.

Introduction

Circuits that control movement are made up of distinct classes of inhibitory and excitatory interneurons synaptically connected to motor neurons (MNs) in the ventral spinal cord (Brown, 1981). Many neurons within locomotor circuits arise from a common precursor pool of multipotential neuroepithelial cells (Leber et al., 1990) but are subsequently distinguishable by cell body position and pattern of gene expression. In particular, MNs coalesce to form columns along the body axis, each characterized by a discrete mediolateral location within the spinal cord, a distinct axonal projection pattern, and the expression of a specific set of LIM-homeodomain (LIM-HD) transcription factors (Tsuchida et al., 1994; Varela-Echavarría et al., 1996). Similarly, interneurons become arrayed in nonoverlapping groups along the dorsoventral axis, each type having discrete axonal projections and gene expression patterns. These distinctive properties of MNs and interneurons are thought to be determined earlier as progenitor cells respond to inductive signals; however, the intrinsic agents activated by these factors remain largely uncharacterized.

The ventral neural tube is primarily patterned through

the concentration-dependent activity of Sonic hedgehog (Shh) (Ericson et al., 1997). Progenitor cells within the ventricular zone interpret their positions in the Shh gradient, expressing factors that circumscribe discrete domains of cell fate specification, such as Pax6 (Ericson et al., 1997), Nkx2.2 (Briscoe et al., 1999), and members of the Gli family (Hui et al., 1994). Specifically, Nkx2.2⁺ progenitors appear to produce dorsal exiting MNs (d-MNs) and a class of ventral interneurons (V3), whereas Pax6⁺ progenitors give rise to ventral projecting MNs (v-MNs) and a number of distinct interneuron types (V1, V2) (Ericson et al., 1997; Sharma et al., 1998). In an analogous fashion, the dorsal neural tube is patterned by tumor growth factor β (TGF β) family molecules, including the bone morphogenetic proteins (BMPs) and activin, that initiate the specification of dorsal neuronal classes (Lee et al., 1998).

Many of the transcription factors marking MN and interneuron classes have been suspected to control cell fate specification, yet most are encountered in multiple cell types, including both interneurons and MNs (Tanabe and Jessell, 1996; Pfaff and Kintner, 1998). For example, the LIM-HD factors Lhx3/4, known to promote the v-MN cell fate, are present in precursors for both v-MNs and V2 interneurons (Sharma et al., 1998) and can drive expression of the V2 gene *Chx10* in ectopic contexts (Tanabe et al., 1998). Thus, it is unclear how an MN utilizes these factors to establish its identity while avoiding the interneuron characteristics they might confer. More generally, this question applies to cell fate determination throughout the nervous system, where the appearance of regional boundaries and specific cell types is frequently accompanied by the expression of multiple transcriptional regulators in overlapping patterns (Rubenstein and Beachy, 1998).

To elucidate how cells discriminate between competing MN and interneuron cell fate-promoting influences, we have focused on the function of HB9, a homeodomain protein with specificity for developing MNs (this report; Harrison et al., 1994; Pfaff et al., 1996; Saha et al., 1997; Tanabe et al., 1998). Though divergent from other members of the homeodomain family, HB9 is widely conserved among vertebrates and is associated with hereditary sacral agenesis (HSA) in humans (Ross et al., 1998). HB9 contains an alanine- and proline-rich N-terminal end but otherwise lacks recognizable motifs that could provide mechanistic insight into its activity. Recently, studies in chick embryos have implicated *CHB9* and its close homolog, *cMNR2*, in MN differentiation (Tanabe et al., 1998). *cMNR2* is expressed in presumptive somatic MN progenitors but is superseded by *CHB9* and the LIM-HD factor *Isl1* as these cells become postmitotic MNs. Misexpression of either *CHB9* or *cMNR2* in dorsal *Isl1*⁺ interneurons causes these cells to differentiate into MNs. Thus, HB9 class factors likely contribute to the specification of MNs, but whether they are necessary for this process remains to be determined.

In this study, we have examined the expression of HB9 in mouse to clarify its role in mammalian MN development. Our studies find that mouse HB9 is expressed

† To whom correspondence should be addressed (e-mail: pfaff@salk.edu).

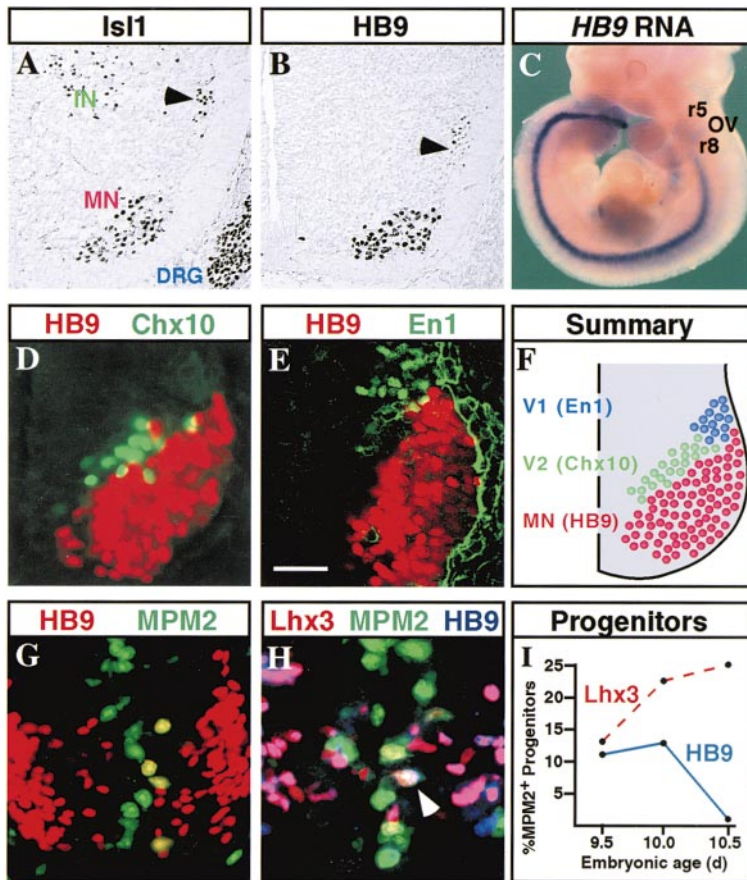


Figure 1. HB9 Is Expressed Exclusively in MNs throughout Development

(A–B) Expression of *Isl1* (A) and *HB9* (B) in E13.5 mouse thoracic spinal cord. While *Isl1* is present in MNs, dorsal interneurons, and DRG sensory neurons, *HB9* is found only in MNs, including visceral preganglionic cells (black arrowhead).

(C) Whole-mount in situ hybridization on an E10.5 mouse embryo detects *Hb9* RNA in a stripe of MNs extending from r8 to the tail. A small group of cells in r5, just above the otic vesicle, also expresses *Hb9* RNA (difficult to detect here).

(D and E) *HB9*, *Chx10*, and *En1* expression in E10.5 mouse thoracic spinal cord. *HB9* is not coexpressed with markers of V2 (*Chx10*), V1 (*En1*), or any other interneurons (data not shown). The MN specificity of *HB9* expression persists in postnatal life (P10; data not shown).

(F) Schematic displaying the expression profile and topographic location of ventral cell types in E10–E11 mouse spinal cord.

(G–I) Analysis of *HB9* in MN progenitors.

(G) *HB9* is present in *MPM2*-marked M-phase progenitors in the ventral spinal cord at E9.5. (H) Triple-label immunofluorescence in E9.5 mouse ventral spinal cord shows that *HB9*⁺ progenitors represent a subset of the *Lhx3*⁺ progenitor pool (white arrowhead, triple-labeled cell). These cells also express *Lhx4* (data not shown).

(I) Quantification of *HB9* and *Lhx3* progenitors in mouse spinal cord from E9.5 to E10.5. Each data point is representative of 500 progenitors counted from six to eight embryos. The presence of *HB9* in *MPM2* cells correlates with

with the peak of MN generation (E9.5–E10). The number of *Lhx3* progenitors increases over time, reflective of the primary period of V2 interneuron generation (E10–E11).

Scale bar, 60 μ m (A and B), 25 μ m (D, E, and H), and 30 μ m (G).

in both MN progenitors and postmitotic MNs, a pattern that approximates a composite of both *HB9*-related genes in chick. All v-MNs express *HB9*, though protein levels vary within individual MN subclasses. In contrast, d-MN classes of hindbrain and midbrain MNs never express *HB9* during the course of their development.

The MN-specific expression pattern of *HB9* and its capacity to promote MN differentiation in the chick advance the hypothesis that *HB9* may be an essential component of the *Shh*-induced MN specification pathway. To address this possibility, we have examined mice with a null mutation targeted in the *Hb9* gene (K. H. et al., submitted). Cells with many characteristics of embryonic MNs develop in these knockouts (KOs) but aberrantly express genes ordinarily restricted to V2 interneurons. The uncoupling of the regulatory mechanisms that separate interneuron and MN genetic programs is accompanied by dramatic effects on MN axonal projections and topological derangements of motor columns. Thus, *HB9* is critical for the proper specification of MNs during development. The repressive function of *HB9* in MNs represents one broadly applicable strategy for obtaining distinct functional readouts from the combinatorially arrayed transcription factors used for cell fate specification.

Results

HB9 Expression in Developing MNs

Previous studies in *Xenopus* and chick embryos suggested that *HB9* might be an MN-specific homeodomain transcription factor (Saha et al., 1997; Tanabe et al., 1998). We determined the expression pattern of *HB9* during mouse embryogenesis to further characterize its potential role in modulating MN development. Initially, we compared its expression with that of LIMHD factor *Isl1*, a gene critical for MN differentiation (Pfaff et al., 1996). *Isl1* marked MNs, dorsal interneurons, and dorsal root ganglion (DRG) sensory neurons, whereas *HB9* was observed only in MNs (Figures 1A and 1B). Both *Isl1* and *HB9* were found in somatic (skeletal muscle-innervating) and visceral (sympathetic ganglion-innervating) spinal MNs (Figures 1A and 1B). *HB9* protein was restricted to MNs, as no coexpression with *En1* (V1 interneurons), *Chx10* (V2 interneurons), or any other interneuronal marker was observed (E9.5–P10; data not shown) (Figures 1D–1F). These results, combined with the cholinergic status and ventral axonal projection of *HB9*⁺ cells (data not shown), demonstrate the MN specificity of *HB9* in the mouse. Outside the nervous system, *HB9* was detected in the notochord and visceral endoderm at embryonic day 8.5 (E8.5) and remained present in these

structures throughout prenatal development (data not shown).

If mouse HB9 is critically involved in MN determination, two predictions arise concerning its expression pattern. First, a general MN differentiation factor would be expected to be found in most or all MNs, irrespective of subtype, and second, the onset of expression should correlate with the timing of differentiation decisions. Regarding the former, HB9 was observed in all hindbrain and spinal cord MNs characterized by a ventral axonal projection (v-MN) (Figure 1C; data not shown). Nevertheless, HB9 expression was limited in two ways: no RNA or protein was detected above the level of the abducens (VI) motor nucleus in rhombomere 5 (r5) despite the presence of v-MNs in the midbrain (Figure 1C), and HB9 was never observed in d-MN groups, such as the spinal accessory (XI) or vagus (X) (Figure 1C, gap between r5 and r8; data not shown). Thus, HB9 expression is found specifically in the MN types (i.e., v-MNs) that arise from *Lhx3/4*⁺ progenitors (Sharma et al., 1998).

The initiation of HB9 expression does appear to correlate with the determination of MN identity. By E9.5, at the onset of MN birth, HB9 became expressed in a subset of ventral progenitor cells distinguished by the coexpression of *Lhx3* and the M-phase marker MPM2 (Figures 1G–1I). From E9.5 to E10, HB9 was detected in 11%–12% of ventral M-phase cells (Figure 1I), a proportion comparable to the ~10% of MPM2 cells expressing the chick MN progenitor marker *cMNR2* (Tanabe et al., 1998). Over the same span, *Lhx3*/MPM2 cells increase from 13% to 23% of the ventral progenitor pool, reflective of a substantial augmentation by V2 interneurons generated after E10. HB9⁺ and *Lhx3*⁺ progenitors were likewise detected in cells pulse labeled with bromodeoxyuridine (BrdU) (data not shown).

Several arguments support the notion that HB9 is present in MNs during the period of differentiation decisions. First, HB9 is expressed in a subset of *Lhx3/4* progenitors, the precursors of v-MNs and V2 interneurons. The presence of HB9 in progenitors precedes the birth of V2 interneurons and correlates with the peak of MN generation (~E10) (Nornes and Carry, 1978). More importantly, HB9 is found in all MNs during the period in which *Lhx3/4* appear to specify the v-MN fate (i.e., from late mitotic stages to the beginning of cell migration) (Sharma et al., 1998). Finally, the early expression of HB9 was independently confirmed in *Isl1*-deficient embryos (data not shown), in which postmitotic MNs fail to develop (Pfaff et al., 1996).

To summarize, HB9 is expressed in presumptive v-MN progenitors at the time of MN birth (E9.5–E10.5) and is maintained in all postmitotic v-MNs of the spinal cord and hindbrain. This pattern roughly encompasses the expression domains of the exclusively postmitotic *cHB9* and the progenitor-specific *cMNR2* and, more importantly, overlaps with the transitory period of *Lhx3/4* expression in all v-MN classes.

To rule out the confounding possibility that our immunological reagents detected multiple HB9-like proteins (such as a mouse *cMNR2* homolog), we tested their reactivity on HB9-deficient mouse embryos created by gene targeting (described below; K. H. et al., submitted). Both a broadly reactive N-terminal antibody (detecting *cMNR2*, *cHB9*, and *mHB9*) and an *mHB9*-specific

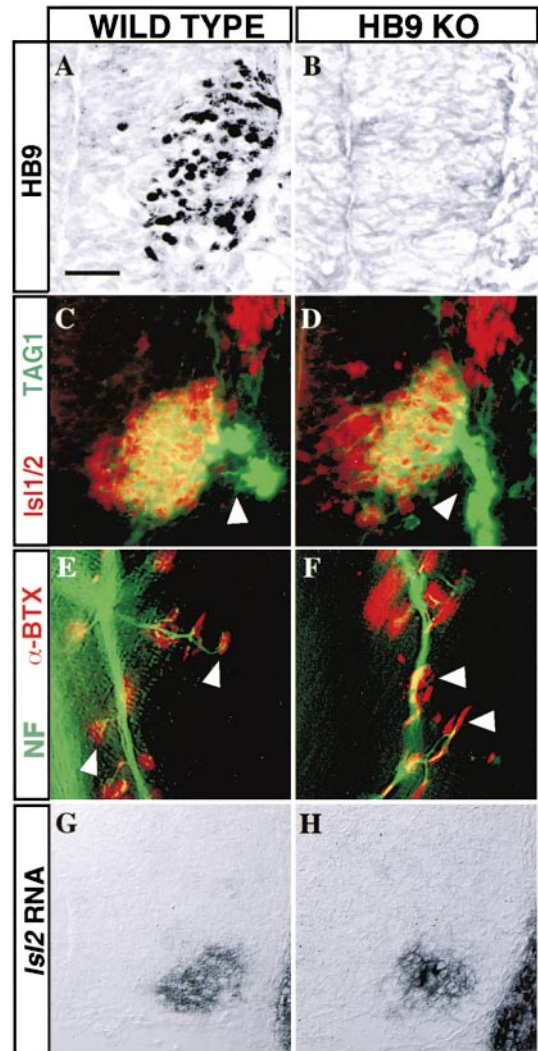


Figure 2. General MN Development Appears Normal in *Hb9* KO Embryos

(A and B) Immunocytochemical localization of HB9 using an N-terminal antibody in E9.5 mouse spinal cord confirms the absence of HB9 protein (and its close homologs) in KO embryos.

(C and D) Immunocytochemical localization of *Isl1/2* and the axonal marker TAG1 in E10.5 mouse thoracic spinal cord demonstrates that MNs are generated in the ventrolateral quadrant of the spinal cord and extend axons through a ventral root (white arrowhead) in wt and *Hb9* KO embryos.

(E and F) Neurofilament (NF) and α -BTX label neuromuscular synapses between E18.5 mouse intercostal nerves and muscles. Both wt and *Hb9* KO embryos contain numerous NMJs visible at the tips of axonal arbors (white arrowheads).

(G and H) In situ localization of *Isl2* RNA in the right ventrolateral quadrant of E13.5 mouse thoracic spinal cord. *Isl2* expression in the *Hb9* KO resembles that of the wt, precluding a wholesale somatic (*Isl2*⁺) to visceral (*Isl2*⁻) MN fate conversion. Visceral MNs are also generated in *Hb9* KO and wt embryos (Figures 6G and 6H; data not shown).

Scale bar, 30 μ m (A and B), 25 μ m (C and D), and 60 μ m (G and H).

C-terminal antibody failed to label nuclei in HB9 KOs (Figures 2A and 2B; data not shown). Thus, any *Hb9*-related gene in mouse is either highly dissimilar to *Hb9* or is dependent upon HB9 for its expression. These

possibilities notwithstanding, HB9 is clearly expressed in mouse MN progenitors and young postmitotic MNs, suggesting that a divergence in HB9 activity may have occurred during the evolution from avians to mammals.

Generation of *Hb9* KO Mice

The precise v-MN specificity of HB9 expression and the demonstration of an MN fate-promoting activity in its close avian homologs (Tanabe et al., 1998) provided the impetus to generate mutant mice that would elucidate the role of HB9 in MN differentiation. We established an embryonic stem cell line heterozygous for *Hb9* by engineering a deletion encompassing the C-terminal half of the protein, including ten amino acids of the homeo-domain (K. H. et al., submitted). This mutation eliminated HB9 protein, as the N-terminal antibody failed to label cells in homozygous mutant embryos (see Figures 2A and 2B). While heterozygous mice were fit and fertile, homozygous null animals died at birth from respiratory paralysis (see below). Though neither heterozygous nor homozygous animals exhibited structural or skeletal abnormalities reminiscent of HSA (data not shown), a human disease associated with *HB9* haploinsufficiency (Ross et al., 1998), the homozygotes did manifest defects in pancreatic development (described in K. H. et al., submitted).

We envisioned several potential consequences of removing HB9 from the MN differentiation pathway. First, few or no MNs might be generated, possibly with a concomitant conversion to an interneuron fate. Second, MNs might develop but fail to complete their proper subtype specification, leading to MN subtype conversions akin to those observed in *Pax6* and *Lhx3/4* KOs (Ericson et al., 1997; Osumi et al., 1997; Sharma et al., 1998). Third, MNs might proceed through a late stage of differentiation at which point they would fail to target properly or form functional connections. Finally, the absence of HB9 from the notochord might result in general dorsoventral patterning abnormalities that could masquerade as any of the aforementioned phenotypes (Chiang et al., 1996). To rule out this last possibility, we examined the *Shh*-responsive patterning genes, *Gli1*, *Gli2*, *Gli3*, *HNF-3 β* , *Nkx2.2*, and *Pax6*, and observed no differences between wild-type (wt) and KO embryos (data not shown).

MNs Are Generated in *Hb9* KO Embryos but Display Abnormal *Isl1* Expression

Initially, we addressed the issue of a complete block to MN development by examining general MN characteristics. The localization in early embryos of the cell adhesion molecule transient axonal glycoprotein 1 (TAG1) on the cell bodies and axons of *Isl1*⁺ neurons projecting from the ventral spinal cord (Figures 2C and 2D) and the association of muscle acetylcholine receptor clusters with nerve terminals in late embryos (i.e., neuromuscular junctions [NMJs]) (Figures 2E and 2F) confirmed the presence of MNs in *Hb9* KOs. Furthermore, *choline acetyltransferase* (*ChAT*) and *Isl2*, selective MN genes within the spinal cord, were detected in both wt and KO embryos (Figures 2G and 2H, *ChAT* not shown). These markers demonstrate that HB9 is dispensable for the generation of MNs; moreover, they exclude the possibility of a wholesale MN subtype conversion in KO embryos

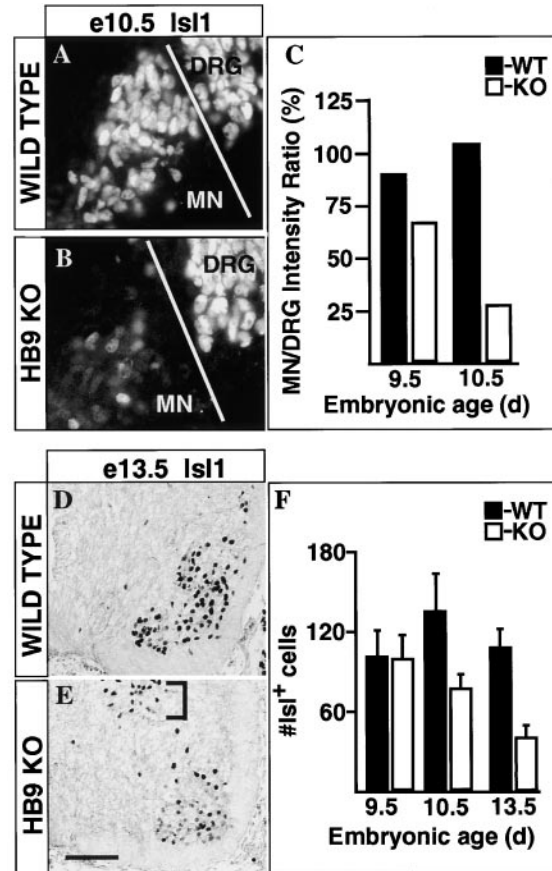


Figure 3. Loss of HB9 Results in Reduced *Isl1* Expression and *Isl1*⁺ Cell Number

(A–C) *Isl1* staining in E10.5 mouse spinal cord used for analysis in (C) (actual measured images undersaturated to linear range of signals).

(C) Quantification of *Isl1* staining represented as a percentage ratio of the mean pixel intensity in individual MNs and DRG neurons ($n > 25$). While *Isl1* levels are fairly equivalent in wt DRG neurons and MNs (MN/DRG = 90%–100% from E9.5 to E10.5), *Isl1* expression is clearly reduced in the MNs of *Hb9* KOs (MN/DRG = 25%–67% from E9.5 to E10.5). Data were consistent in 10 wt and KO embryos analyzed.

(D–F) Analysis of *Isl1* cell number in mouse spinal cord from E9.5 to E13.5.

(D and E) Representative immunohistochemistry of *Isl1* in the E13.5 brachial spinal cord used to count cell number in (F). Bracket in (E) denotes *Isl1*⁺ interneurons excluded from this analysis.

(F) Quantification of *Isl1*⁺ cell number at brachial levels from E9.5 to E13.5 represented as mean number of *Isl1*⁺ cells \pm SD in the ventrolateral quadrant of a 10 μ m thick section. At least ten sections are analyzed for each time point. Whereas the number of *Isl1*⁺ cells is similar in E9.5 wt and KO embryos, by E13.5, a reduction in *Isl1*⁺ cell number is apparent in KO embryos.

Scale bar, 25 μ m (A and B) and 60 μ m (D and E).

from v-MN (*Isl2*⁺/TAG1 in ventral root) to d-MN (*Isl2*⁻/TAG1 in dorsal root) (Figures 2C and 2D) or from somatic (diaphorase⁻/*Isl2*⁺) to visceral (diaphorase⁺/*Isl2*⁻) (Figures 2G and 2H, diaphorase not shown).

In the course of the foregoing analysis, it became apparent that differences in *Isl1* expression existed between MNs in KO and wt embryos. As MNs were born at E9.5 in wt and KO embryos, *Isl1*⁺ cell number appeared fairly equivalent (Figure 3F), but protein levels

were reduced by 25% in KO embryos (Figure 3C); indeed, as development proceeded, the disparity between wt and KO embryos increased with a diminution of both *Isl1*⁺ cell number and expression level in KO animals (Figure 3). Despite the gradual extinction of *Isl1* expression in MNs from E9.5 to E13.5, no increase in cell death measured by TUNEL labeling was observed in KO embryos (data not shown). Thus, our results suggest that MNs lacking HB9 are subject to the loss of *Isl1*, perhaps en route to a fate conversion.

V2 Interneuron Genes Are Expressed in MNs Lacking HB9

As described above, HB9 is precisely compartmentalized to MNs both at early and late stages of their differentiation and thus may be expected to control a fate decision between MN and interneuron. Consistent with this possibility, HB9 class factors misexpressed in the chick cause dorsal interneuron progenitors to differentiate as MNs and interneuron-specific genes to be downregulated (Tanabe et al., 1998). This suppression of interneuron-specific gene expression may stem from the interference created by MN programs initiated in interneurons, a precarious conclusion given the dispensability of HB9 for MN generation. Alternatively, HB9 may possess a direct interneuron-repressive activity. To assess this latter proposition, we examined the expression of interneuron genes in KO and wt embryos. We used *Chx10* and *Lhx3/4* as markers of V2 interneurons; *En1*, of V1 interneurons; *Lhx1*, of intermediate zone (IZ) interneurons; *Sim1*, of V3 interneurons; and *Brn3.0* and *Lhx2*, of dorsal interneurons. Wt and KO embryos expressed similar profiles of interneuron markers (Figures 4A and 4B; data not shown) except that KOs betrayed a striking dysregulation of V2 interneuron genes in MNs (Figures 4C–4F; Table 1).

In wt embryos, V2 interneurons initially express *Lhx3/4* as they leave the cell cycle, followed subsequently by *Chx10* in the postmitotic cells (Figures 4C and 4E). *Lhx3/4* are also transiently expressed in all v-MNs but are downregulated as the cells migrate laterally (Figure 4C). In contrast, *Hb9* KO embryos manifested significant upregulation of *Lhx3/4* and *Chx10* within MNs (Figures 4D and 4F). *Lhx3/4* were detected in ~90% of the *Isl1*⁺ MNs at E10.5, whereas these factors were present in only 27% of the *Isl1*⁺ MNs in wt embryos (Figures 4C and 4D; Table 1). Similarly, the V2 marker *Chx10* was observed in 36% of the *Isl1*⁺ cells in *Hb9* KO embryos, while wt MNs never expressed this factor (Figures 4E and 4F; Table 1). By E13.5, the *Isl1*⁺ cells expressing *Chx10* declined in *Hb9* KOs to 14%, revealing a dynamic relationship between *Isl1* and *Chx10* (Table 1). In part, the reduction in *Chx10*⁺/*Isl1*⁺ colabeling appeared to result from the extinction of *Isl1* from ~50% of the MNs in *Hb9* KOs (Figures 3D–3F).

The selective upregulation of V2 interneuron genes in *Hb9* KO embryos revealed a potential developmental link between MNs and V2 neurons, consistent with the early presence of *Lhx3/4* in both classes. The attendant change in the pattern of *Isl1* expression suggested the possibility of a fate conversion of MNs to V2 interneurons.

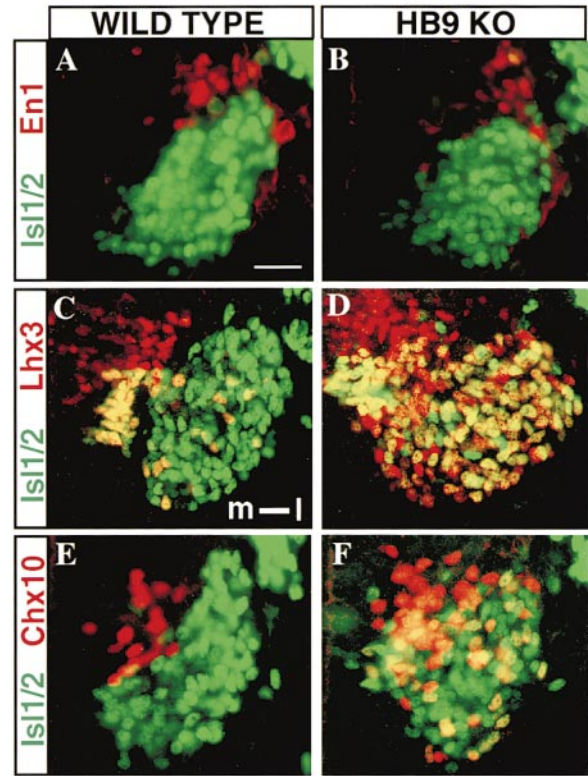


Figure 4. HB9 Prevents Inappropriate V2 Interneuron Gene Expression within MNs

(A–F) Double-label immunohistochemistry of MN and interneuron genes in E10.5 thoracic spinal cord. No coexpression of *En1* (A and B) with *Isl1/2* is observed in wt or KO embryos. The populations of V1 (A and B), V3, IZ (data not shown), and dorsal interneurons (data not shown) are generated in equivalent number and position in both wt and KO embryos.

(C and D) Expression of *Lhx3*, a marker of medial MNs and V2 interneurons, is inappropriately maintained in lateral MNs of *Hb9* KO embryos. Compass in (C) indicates mediolateral axis orientation (m–l).

(E and F) Numerous *Isl1*⁺/*Chx10*⁺ cells are found in *Hb9* KO but not wt embryos. V2 markers, *Lhx3/4* and *Chx10*, continue to be misexpressed in the *Isl1*⁺ cells of E13.5 *Hb9* KOs (see Table 1). Images are representative examples from 40 wt and KO embryos analyzed.

Scale bar, 20 μm (A–F).

Cell-Type Specific Markers and Neuronal Phenotype Are Dissociated in *Hb9* KOs

To assess a potential fate conversion of MNs to interneurons, we developed a lineage-tracing strategy to follow “would-be” HB9⁺ cells in *Hb9* KO embryos. The upstream promoter region of the mouse *Hb9* gene (Arber et al., 1999 [this issue of *Neuron*]) was integrated into the 3′-untranslated region of the *Isl2* locus and used to drive LacZ expression in HB9⁺ spinal cord cells (*Hb9lacZ*;wt and *Hb9lacZ*;KO mice). The LacZ label recapitulated HB9 expression in spinal MNs (Figure 5A) and was found to persist in *Hb9lacZ*;KO embryos (Figure 5B); hence, HB9 was not required for the expression of the *Hb9lacZ* transgene. The fate of MNs in *Hb9* KO embryos could thus be traced by virtue of the LacZ lineage marker. As expected, many LacZ⁺ cells were found coexpressing V2 markers, such as *Chx10*, in *Hb9lacZ*;KO embryos (Figure 5B; Table 1).

Table 1. Marker Expression during Spinal Cord Development

Markers		E9.5		E10.5		E13.5	
		wt	KO	wt	KO	wt	KO
Isl1/Lhx3	Number of cells	77 ± 21	103 ± 13	36 ± 9	70 ± 5	25 ± 6	23 ± 7
	Percentage of total Isl cells	69%	93%	27%	90%	23%	41%
Isl1/Chx10	Number of cells	0	2 ± 1	0	28 ± 9	0	8 ± 3
	Percentage of total Isl cells		2%		36%		14%
LacZ/Chx10	Number of cells	0	2 ± 1	0	45 ± 7	0	33 ± 4
	Percentage of total LacZ cells		2%		50%		39%

Double-label immunocytochemistry at brachial spinal cord levels of *Hb9lacZ;wt* and *Hb9lacZ;KO* embryos was used to quantify gene expression at E9.5, E10.5, and E13.5. Values represent the mean number of double-label cells ± SD in the ventrolateral quadrant of a 10 μm thick section. Each value from >15 sections is representative of >10 embryos examined. Lhx3 is detected in nearly all MNs of KOs from E9.5 to E10.5. Chx10, only observed in the MNs of KO embryos, displays a dynamic expression pattern peaking between E10.5 and E11.5.

Triple-label immunofluorescence was used to monitor the expression of Isl1 and Chx10 in LacZ⁺ lineage-marked cells. In *Hb9lacZ;KO* embryos, Chx10 was detected in LacZ⁺ cells that varied in their Isl1 status from strongly positive to negative (data not shown). The identification of LacZ⁺/Chx10⁺/Isl1⁻ cells in *Hb9lacZ;KOs* bolstered the proposition that MNs had adopted a V2 interneuron fate. To directly determine neuronal phenotypes in these embryos, we labeled MNs and interneurons using retrograde ventral root fills and retrograde

intraspinal fills, respectively. To our surprise, LacZ⁺/Chx10⁺/Isl1⁻ cells in *Hb9* KOs could be labeled from the ventral root (Figures 5C and 5D; LacZ data not shown), suggesting these would-be HB9⁺ cells possess MN projections despite their interneuron marker profile. Correspondingly, the labeling of interneurons by injection of rhodamine-dextran into the spinal cord failed to mark LacZ⁺/Chx10⁺/Isl1⁻ cells, though it did identify endogenous V2 interneurons expressing only Chx10 (Figures 5E and 5F; Isl1 data not shown). These results clearly

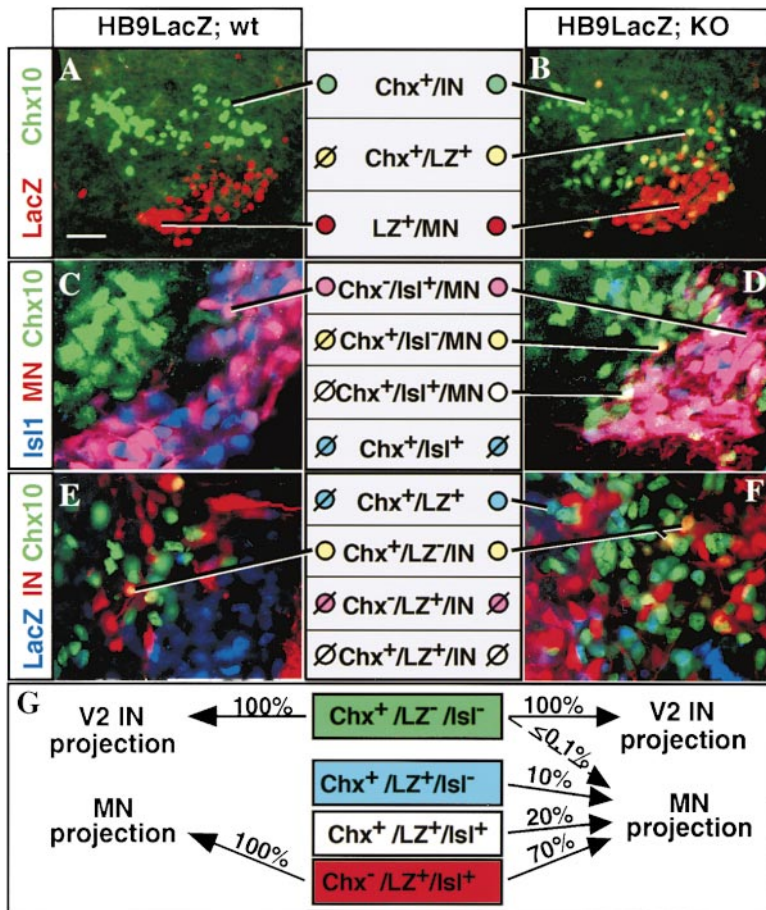


Figure 5. MNs Misexpressing V2 Interneuron Genes Retain MN-Like Axonal Projections

(A and B) Localization of LacZ and Chx10 in E13.5 mouse thoracic spinal cord. LacZ recapitulates HB9 expression in MNs and is robustly expressed in *Hb9lacZ;KO* embryos, demonstrating that the promoter is active in the absence of HB9. Numerous LacZ⁺/Chx10⁺ cells are observed in *Hb9lacZ;KO* but not in *Hb9lacZ;wt* embryos. Center panels indicate examples of each cell type: Isl, Isl1; Chx, Chx10; LZ, LacZ; and φ, no cells detected. See Table 1 for quantitation.

(C and D) Analysis of axonal projections in E12.5 mouse using retrograde labeling by rhodamine-dextran placed in the ventral root (MN). MNs in wt express Isl1 (magenta to purple) but not Chx10 (green), while MNs in KO express Chx10 (yellow), Isl1 (magenta), or both (white).

(E and F) Interneuron (IN) cell bodies in E13.5 mouse localized by intraspinal cord labeling with rhodamine-dextran. Distinct classes of interneurons, but no MNs, are labeled by this technique. While Chx10⁺ interneurons (yellow) can be backlabeled in wt and KO embryos, no Chx10⁺/LacZ⁺ (white) or Chx10⁻/LacZ⁺ (magenta) interneurons are observed. Note that Chx10⁺/Isl1⁺/LacZ⁺ cells do not project as interneurons, only as MNs (see [G] for summary). Scale bar, 25 μm (A and B) and 15 μm (C–F).

(G) Summary diagram of gene expression patterns and axonal projections with approximate percentages indicated over arrows. *Hb9* KOs (right side) contain MNs (defined by axonal projection) of normal genetic profile (Chx10⁻/Isl1⁺/LacZ⁺) and MNs that misexpress V2 interneuron genes (Chx10⁺/Isl1⁺/LacZ⁺ and rare Chx10⁺/Isl1⁻/LacZ⁺). Both wt (left) and KO embryos contain only one class of V2 interneuron, Chx10⁺/Isl1⁻/LacZ⁻.

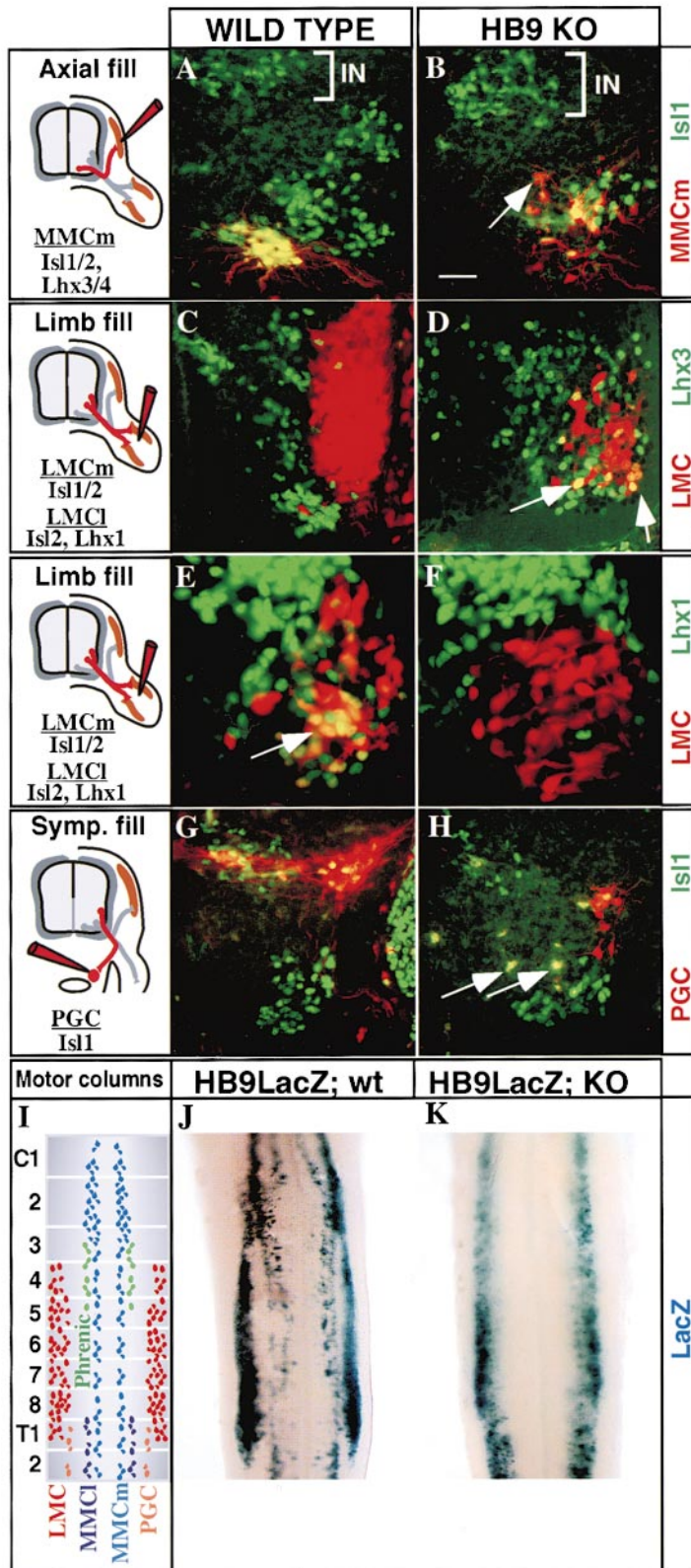


Figure 6. *Hb9* KO MNs Display Aberrant Gene Expression and Severe Disorganization of Columnar Topology

(A–H) Retrograde labeling of specific motor columns using rhodamine-dextran. Schematics displaying placement of dye and normal LIM gene expression patterns are found to the left of each set of panels. Sections shown are E13.5 brachial (A and B), E13.5 lumbar (C and D), E10.5 lumbar (E and F), and E13.5 thoracic (G and H).

(A and B) At E13.5, dextran placed in dorsal axial muscles labels the medial (m) half of the median motor column (MMCm), seen in wt as a small discrete cluster of Isl1⁺ cells. These cells lie directly ventral to Isl1⁺ interneurons (indicated by white bracket). KO embryos show scattering of MMCm cell bodies to more lateral and dorsal positions (note relationship of labeled cells to Isl1 interneurons). Some cells do not express Isl1 (white arrow).

(C and E) Dextran placed in the limb backlabels the lateral motor column (LMC), the lateral (l) half of which normally expresses Lhx1 (white arrow in [E]) but not Lhx3. (D and F) *Hb9* KO embryos upregulate Lhx3 in their scattered LMC (white arrows, [D]) and lose Lhx1 expression (F).

(G and H) Retrograde labeling of preganglionic sympathetic MNs (PGC) by dextran placed in the chain of thoracic sympathetic ganglia. The Isl1⁺ PGC is located in a dorsal position (above V2 interneurons) in wt embryos, while KOs show a moderate scattering of the column (white arrows) and a substantial reduction in its size.

(I) Graphic representation of motor columns at E13.5 in wt mouse cervical (C1–C8) to thoracic (T1–T2) spinal cord. The diagram is in register with the spinal cords displayed in (J) through (K).

(J and K) X-gal staining on E14.5 spinal cords of *Hb9lacZ;wt* and *Hb9lacZ;KO* embryos in ventral view. Wt embryos display strong staining in a large lateral column (LMC) extending from C4 to T1, while the median column (MMC) extends the entire length (shown here from C1 to T2). In KO embryos, all X-gal stained cells are found in a midlateral position, with no distinction between columns. The single column appears to shift medially at C8–T1.

X-gal stains and fills were performed on 40 embryos from six litters in each case. Abbreviations: MMC, median motor column; LMC, lateral motor column; and PGC, preganglionic motor column. The columns are further subdivided into medial (m) and lateral (l) halves. Scale bar, 25 μm (A–D, G, and H) and 15 μm (E and F).

demonstrate that cells fated to become MNs (marked by LacZ) acquired a variety of genetic profiles, including the profile of V2 interneurons; despite their gene expression patterns, however, these cells appeared to project axons from the neural tube, like MNs (Figure 5G).

MN Cell Body Topology Is Disorganized in *Hb9* KOs

No fate conversion occurred in KO embryos, rendering uncertain the functional consequences that result from the perturbation of gene expression in MNs. Despite

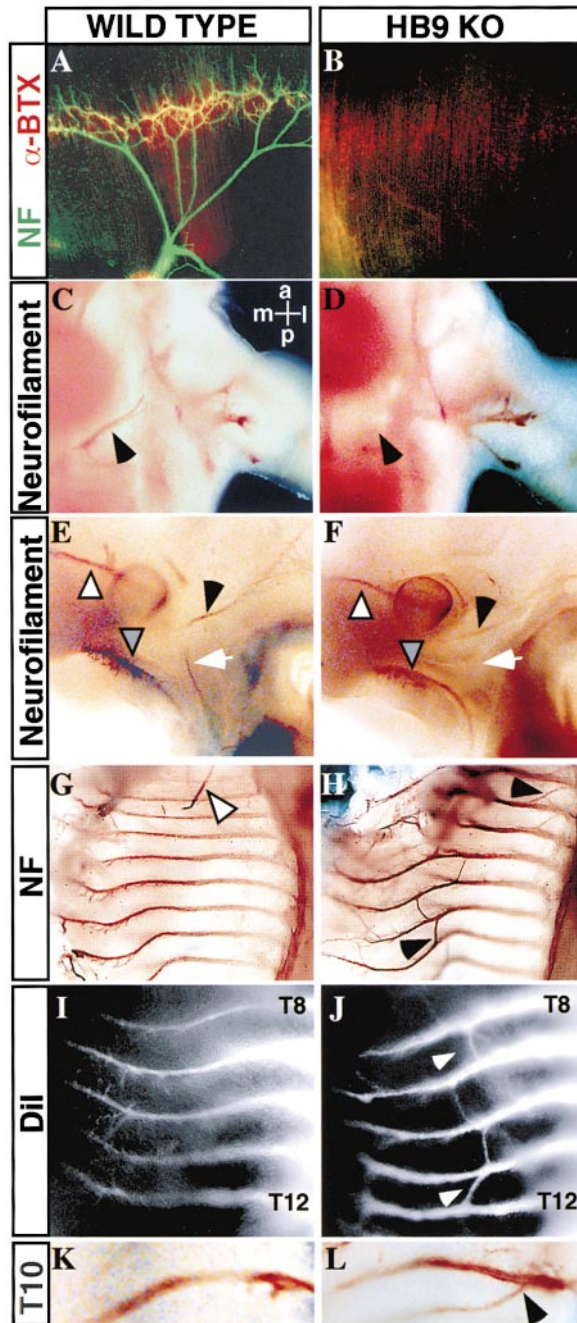


Figure 7. HB9 Is Essential for Proper Axonal Projections in Specific MN Groups

(A and B) Whole-mount staining of E16.5 diaphragm muscle with neurofilament antibody (NF) and Texas red-conjugated α -BTX localizes NMJs at the tips of phrenic nerve arbors. KO embryos show a complete absence of the phrenic nerve, with scattered acetylcholine receptor clusters visible. No motor innervation of the diaphragm is seen at any age examined (E12.5–E18.5, four to six embryos at each age).

(C–F) Whole-mount immunostaining of E11.5 embryos with neurofilament antibody reveals axonal architecture.

(C and D) Close-up view of the ventral forelimb axillary region reveals the absence in the KO of the phrenic nerve (black arrowhead) from the point at which it leaves the brachial plexus. Compass in (C) indicates anteroposterior (a–p) and mediolateral (m–l) axes.

(E and F) Nerves innervating the peri-orbital region of the head include the maxillary (gray triangle) and ophthalmic (white triangle) branches

of hybrid characteristics, HB9-deficient MNs displayed relatively normal neurotransmitter phenotype, axon extension from the neural tube, and NMJ formation (see above). However, retrograde labeling of specific MN subtypes by injecting rhodamine-dextran into discrete peripheral targets (Figure 6 schematics) revealed striking defects in MN organization. Normally, motor columns become topologically aligned by E13.5 as individual MN subtypes settle into stereotyped locations within the spinal cord (Figure 6I). The backlabels revealed a remarkable disorganization of each motor column in *Hb9* KOs (Figure 6). Cell bodies were scattered throughout the ventrolateral horn, with little correlation between topographical location and columnar identity. The intermingling of MNs was further corroborated in *Hb9lacZ*;KO embryos stained with X-gal, in which the segregated columns apparent in *Hb9lacZ*;wt embryos were found to be merged (Figures 6I–6K).

Coincident with their disrupted topology in KO embryos, MNs expressed abnormal combinations of LIM-HD markers in defiance of the usual code (Figure 6 schematics) (Tsuchida et al., 1994). For example, some medial motor column (MMCm) cells lacked *Isl1* (Figures 6A and 6B), while most lateral motor column (LMC) cells demonstrably expressed *Lhx3* but not *Lhx1* (Figures 6C–6F). Though the migration and gene expression defects varied between individual motor columns, all displayed some degree of disorganization. Overall, these results underscore the finding that MN generation is HB9 independent, while proper MN specification requires functional HB9.

MN Axon Guidance Defects in *Hb9* KOs

Our analysis of *Hb9* KO embryos revealed that MNs assume inappropriate columnar positions while expressing atypical arrays of genes (see above). These results raised the possibility that specific MNs project axons erroneously, perhaps from dysregulated pathfinding mechanisms. In particular, we suspected that the nerves of the respiratory apparatus (i.e., phrenic and intercostal nerves) might be severely compromised, thereby producing the observed neonatal lethality of the *Hb9* mutation. NMJ and nerve staining on diaphragm muscle, the target of the phrenic nerve, confirmed the total absence of motor innervation (Figures 7A and 7B). A more direct assessment of axon guidance employing

of the trigeminal (V), the oculomotor (III; black arrowhead), and the abducens (VI; white arrowhead). KO embryos are missing the HB9⁺ abducens. Trigeminal ganglion was removed for clarity.

(G–L) Axonal projections of intercostal nerves revealed in E12.5 mouse embryos.

(G and H) Whole-mount neurofilament stain reveals multiple bridging nerves (black arrowheads) in the thorax of KO but not wt embryos. Note the presence of the phrenic nerve (white triangle, [G]) entering the chest cavity of the wt embryo.

(I and J) Orthograde Dil labeling at thoracic levels reveals that the thoracic bridges (white arrowheads) are motor nerve defects.

(K and L) Orthograde photoconverted Dil label of T10. Wt T10 tracks along the tenth rib without branching, whereas KO T10 shows a proximal branch point (black arrowhead) into the eleventh intercostal nerve path.

At least five embryos from separate litters observed with displayed phenotypes in each instance.

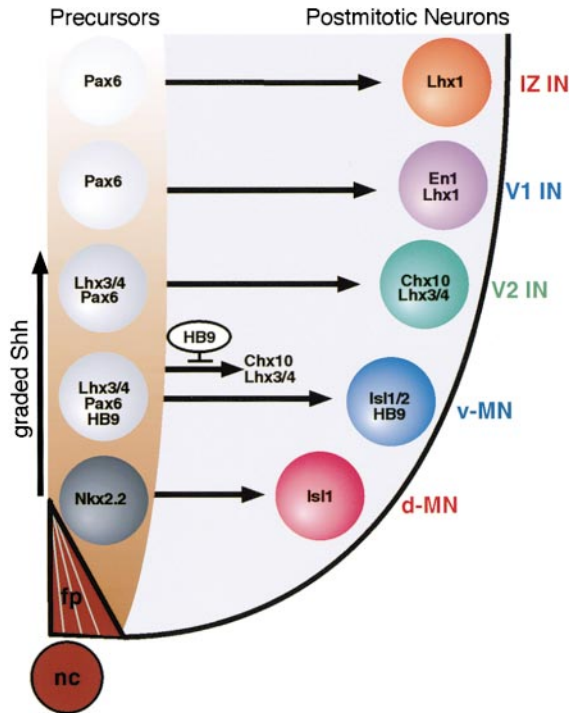


Figure 8. Summary of Murine Ventral Spinal Cord Development
Shh is secreted by the notochord (nc) and floor plate (fp) and acts in a concentration-dependent manner to establish precursor cell populations (gray cells) for postmitotic neuronal types (colored cells). Distinct precursor cell types express unique combinations of homeodomain transcription factors Pax6, Nkx2.2, and Lhx3/4. The precursors for V2 interneurons and v-MNs, however, arise from cells that express a related profile of these factors (Sharma et al., 1998). As v-MNs are born, murine HB9 appears prior to the onset of Isl1 expression. In mice lacking *Hb9*, postmitotic MNs are generated but express V2 interneuron genes such as *Lhx3/4* and *Chx10*. Thus, HB9 appears to modify the transcriptional readout of broadly expressed factors (e.g., *Lhx3/4* and *Pax6*), such that MNs acquire a unique and not hybrid identity. Overall, these results demonstrate that MNs actively suppress inappropriate gene expression in pathways parallel to those controlling differentiation per se.
Abbreviations: IZ IN, intermediate zone interneuron; V1 IN, ventral position 1 interneuron; V2 IN, ventral position 2 interneuron; v-MN, ventral exiting motor neuron; and d-MN, dorsal projecting motor neuron.

whole-mount neurofilament staining (Figures 7C, 7D, 7G, and 7H) and orthograde 1,1'-diiodoacetyl-3,3',3'-tetramethylindocarbocyanine perchlorate (Dil) labeling (data not shown) of segments C3–T1 revealed that in KO embryos, the phrenic nerve might be misrouted into the forelimb, possibly failing to branch from the brachial plexus (Greer et al., 1999). In addition to the phrenic, the abducens (VIth cranial nerve) was absent in *Hb9* KO embryos (Figures 7E and 7F), despite the presence of LacZ⁺ cells in r5 at E10.5 in *Hb9lacZ*;KO embryos (data not shown).

Aside from the deficit of abducens and phrenic nerves in KO embryos, it was uncertain whether any bona fide axon pathfinding errors had occurred. As a simple means of analyzing late peripheral projections, we utilized whole-mount neurofilament staining. At E12.5, KO embryos displayed a striking nerve-bridging phenotype

in the thorax (Figures 7G and 7H). To test if the anastomoses between thoracic nerves were made up of motor axons, a prediction of whether the phenotype was cell autonomous, orthograde Dil labeling of thoracic spinal segments was performed on embryos with the dorsal sensory roots severed. This selective labeling of MNs revealed multiple connections between intercostal nerves at distal points along their trajectories (Figures 7I and 7J). To resolve whether these bridges represented the fusion of collateral branches or the misprojection of axon growth cones, Dil was placed in a single thoracic segment (Figures 7K and 7L). In the *Hb9* KO embryo, a portion of the tenth intercostal nerve meandered into the zone of the eleventh rib, where it coursed along with its unlabeled eleventh nerve counterpart. Thus, some thoracic motor axons make pathfinding errors at cryptic choice points but eventually join extant pathways when encountered. Overall, there was considerable variation in the number and location of intercostal nerve pathfinding defects both between and within single KO embryos, but all displayed some erroneous nerve projection.

In conclusion, HB9 is essential for proper MN specification, mediating directly—or through suppression of inappropriate gene expression—the accurate cell body migration and axon pathfinding of many classes of MNs.

Discussion

The progenitor cells of v-MNs and V2 interneurons express a related profile of genetic markers (Ericson et al., 1997; Sharma et al., 1998), suggesting that the intermediary pathways in the specification of these neurons are intertwined. HB9 is required to resolve the identities of these neurons during development, as KO mice generate hybrid cells with characteristics indicative of both MNs and V2 interneurons. These abnormal cells extend axons from the neural tube, like MNs, but exhibit severe pathfinding defects and fail to segregate topologically within the spinal cord. Thus, HB9 suppresses interneuron genetic programs and facilitates the development of normal patterns of MN connectivity. We discuss the role of HB9 in MN differentiation and consider how the strategies used to establish MN and interneuron identity may relate to the generation of other neuronal classes in vertebrates.

Coordinate Development of MN and Interneuron Subclasses

The specification of cell fates in the ventral neural tube is initiated in dividing progenitor cells by the graded activity of Shh (Figure 8). It is noteworthy that v-MNs and V2 interneurons arise from related *Lhx3/4*⁺ progenitor cells but use different neurotransmitters, synapse with distinct targets, and subserve different biological functions. In addition, both cell types appear dependent on *Lhx3/4* for their specification (Sharma et al., 1998; K. S. et al., unpublished data). Thus, these cells, with their common origin but distinct fates, present an interesting developmental problem: how are *Lhx3/4* utilized to promote two discrete identities without engendering hybrid characteristics through activation of common target genes?

One simple explanation posits the establishment of

cell identity through combinatorial gene expression. Lhx3/4 could cooperate with Isl1, for example, to activate a unique set of v-MN genes (Jurata et al., 1998). However, MNs would still require a mechanism to silence Lhx3/4-driven transcription of V2 interneuron genes. Our data are consistent with HB9 providing this heretofore unsuspected repressive function. HB9 appears in Pax6⁺/Lhx3/4⁺ progenitors at the onset of MN specification by Shh and is maintained postmitotically as the v-MN fate is consolidated by Lhx3/4 and Isl1. Elimination of HB9 results not in an MN-to-interneuron fate conversion but rather in MNs manifesting hybrid characteristics, including the inappropriate expression of V2 interneuron genes. Moreover, there is no evidence for global interneuron gene activation, as other programs remain silent in MNs. Thus, this analysis uncovers an additional layer of complexity in combinatorial specification: MNs can achieve a hybrid state, but this potential intermediate fate is avoided through repression of interneuron programs.

Our observations demonstrate that MNs are inherently capable of expressing genetic programs representative of V2 neurons, a tendency suppressed by HB9. These data further reinforce the view that lineally related cells employ dedicated transcriptional repressors to restrain the potential to express conflicting genetic programs. For example, the *tramtrak* repressor inhibits the expression of R7 photoreceptor cell genes in the closely related cone cells of the *Drosophila* eye (Xiong and Montell, 1993). By the same logic, the absence of HB9 from d-MNs comports with their distinct origin from progenitors unrelated to those of V2 interneurons (Figure 8). d-MNs may lack the intrinsic potential to express V2 genes, obviating the need for the repressive function of HB9.

The Role of HB9 in Motor Axon Guidance and Cell Body Organization

HB9 expression is detected in many subclasses of MNs that project axons to different targets and sort into unique columnar positions within the spinal cord. LIM-HD gene expression is ordinarily found in combinatorial patterns that mark different MN subtypes (Tsuchida et al., 1994; Appel et al., 1995; Thor et al., 1999), but their regulation is altered in *Hb9* KOs. Normally, only MMCm MNs retain Lhx3/4 during axon extension to the dermomyotome, while LMCI MNs express Lhx1 as they innervate the dorsal limb musculature. In HB9-deficient MNs, Lhx3/4 become ectopically expressed, while Lhx1 expression is silenced, yet increased projections to the dermomyotome at the expense of projections to the dorsal limb are not observed (data not shown). These violations of the LIM gene code suggest that the role of these factors in specifying the peripheral axonal projections of MNs requires further characterization.

In addition to the incoherent patterns of LIM-HD gene expression, numerous axon guidance defects exist in *Hb9* KO embryos. Intercostal nerves abnormally cross thoracic segment boundaries, and the phrenic and abducens nerves fail to innervate their diaphragm and extraocular muscle targets, respectively. Although other navigation errors likely occur at normal choice points, they cannot be identified by standard axonal tracing methods because marker gene expression and MN subtype identity are dissociated in *Hb9* KOs. Nevertheless,

retrograde tracing reveals that MN soma have scattered from their stereotyped topological positions within the spinal cord.

Taken together, our data suggest that HB9 is required for many classes of MNs to sort in the spinal cord and extend axons along appropriate pathways. The genes that mediate these processes have yet to be identified, making uncertain the extent of direct contribution by HB9 to the specificity of MN connectivity. HB9 loss of function may result in failure to express target genes that facilitate axon guidance and cell migration. Also plausible, the connectivity errors in *Hb9* KO embryos may arise indirectly from the upregulation of V2 interneuron cell adhesion molecules in MNs. One such example in *Drosophila* involves the disruption of interneuron pathfinding by *Connectin* and *neuroglian* (Siegler and Jia, 1999). Engrailed-mediated repression appears to be required to prevent aberrant upregulation of these adhesion molecules in interneurons.

HB9 Operationally Acts as a Transcriptional Repressor

In *Hb9* KO embryos, virtually all postmitotic v-MNs maintain Lhx3/4, a phenomenon indicative of V2 interneuron gene upregulation in these cells (Figure 8). In addition, Chx10, a definitive V2 marker, is ectopically expressed in v-MNs but appears unstable. This "confused" state is reminiscent of the hybrid neuroectoderm/mesoderm phenotype produced by mutation of the *snail* repressor in *Drosophila* (Hemavathy et al., 1997). Similarly, in zebrafish *floating head* mutants, the loss of Not transcription factor activity leads to transient coexpression of paraxial and axial mesoderm genes (Halpern et al., 1995; Talbot et al., 1995). The hybrid pattern of MN/interneuron marker coexpression is correspondingly dynamic in *Hb9* KOs, possibly an outcome of stochastic interactions between the genetic circuits activated in HB9-deficient MNs. Between E9.5 and E13.5, these marker combinations segregate into different categories, including Isl1⁺/Chx10⁻, Isl1⁻/Chx10⁺, and Isl1⁺/Chx10⁺. Cells of each type project axons from the neural tube, despite the impression created by markers (e.g., Isl1⁻/Chx10⁺) that MNs have converted into interneurons. Nonetheless, our results demonstrate that HB9 operationally acts as a transcriptional repressor, perhaps directly via its alanine-rich segment (Hanna-Rose and Hansen, 1996).

Repressors contribute to patterning mechanisms in a variety of developmental contexts. Broad dorsoventral domains in the spinal cord appear to be established by inductive gradients through the balanced activity of Gli/Ci activators and repressors in a manner analogous to the regionalization of the *Drosophila* blastoderm (Rivera-Pomar and Jackle, 1996; Ruiz i Altaba, 1998). In *Caenorhabditis elegans*, mutations in the *unc-37 groucho*-like corepressor cause VB MN-type presynaptic inputs to form on sister VA MNs (Pflugrad et al., 1997), indicating that transcriptional repressors help establish the distinct identity of these sibling neurons. Similarly, v-MNs and V2 interneurons in vertebrates are closely related cells whose specifications are dependent on the repressive activity of HB9. This function may exist in other interneuron classes, such as Lhx1⁺ V1 interneurons, which are distinguished from Lhx1⁺ IZ interneurons by

the expression of the transcriptional repressor En1 (Figure 8).

Evolution of HB9 Activity: Implications for MN Specification

In humans, hereditary mutations of *HB9* result in HSA due to haploinsufficiency (Ross et al., 1998). One potential etiology of HSA-like phenotypes are notochord defects akin to the zebrafish *no tail* and mouse *Danforth's short tail* mutants (Halpern et al., 1993; Maatman et al., 1997). Although expressed at low levels in the mouse notochord, HB9 appears not to contribute to axial patterning or skeletal development (K. H. et al., submitted). Thus, human and mouse genetics reveal that the function of *Hb9* and/or redundant genes has changed over the course of vertebrate evolution. Comparison of HB9 expression in mouse and chick also reveals significant differences between these species. In mouse, the expression of HB9 initiates early in v-MNs, frequently at the progenitor cell stage, while in chick, the gene is expressed much later in postmitotic MNs (Tanabe et al., 1998). Moreover, chick appears to possess two *HB9*-related genes, yet our immunological reagents failed to detect a second such factor in HB9-deficient mouse embryos. Taken together, our results raise the possibility that like *netrin-1* (Serafini et al., 1996), *Hb9* function in the mouse spinal cord subsumes the activity of two genes in the chick.

The finding that MNs are specified in *Hb9* KO raises the question of how these neurons acquire their appropriate identity. KOs have revealed that many transcription factors, such as *Lhx3*, *Lhx4*, *Pax6*, and *Hoxc8*, contribute to the specification of MN subtype identities, but only *Isl1* appears to be universally required for MN differentiation per se (Pfaff et al., 1996; Ericson et al., 1997; Osumi et al., 1997; Sharma et al., 1998; Tiret et al., 1998). Nevertheless, other factors must cooperate with *Isl1*, for its expression is neither limited to MNs nor sufficient to trigger MN differentiation (Tanabe et al., 1998). Although the nature of the transcriptional code for MN specification remains elusive, the ectopic expression of cHB9 in *Isl1*⁺ interneurons triggers MN differentiation (Tanabe et al., 1998). Thus, in some cellular contexts, repressors of interneuron genes, such as HB9 or MNR2, provide a critical function in modulating the appropriate transcriptional readout for MN specification.

The repressive function described above, potentially applicable to the specification of neuronal identity throughout the developing CNS, may provide one means for neuronal diversity to evolve. Rather than being generated de novo, new subtypes can arise from existing groups by coopting factors and trimming their regulatory profiles (Duboule and Wilkins, 1998; Eizinger et al., 1999). For example, the V2 genes, *Lhx3/4*, may have been adopted by MNs in the evolution of the v-MN lineage (Arendt and Nübler-Jung, 1999). The novel gene combinations thereby generated would require modulation by a repressive activity. Perhaps this may explain why *Hb9* homologs are lacking in *C. elegans*, an organism with few cell types in which LIM-HD factors are expressed very selectively in nonoverlapping patterns (Hobert and Westphal, 1999). Only in organisms such

as *Drosophila* and vertebrates would HB9 be required to distinguish among the diverse developmental outcomes resulting from overlapping LIM-HD expression. More generally, restrictive strategies may cooperate with combinatorial fate determination mechanisms throughout the developing embryo.

Experimental Procedures

Immunocytochemistry and In Situ Hybridization

Immunocytochemistry was performed with the following antibody dilutions: rabbit anti-C-terminal HB9, 1:16,000 (see below); guinea pig anti-C-terminal HB9, 1:10,000 (see below); rabbit anti-N-terminal HB9, 1:8,000 (see below); rabbit anti-*Isl1*, 1:8,000 (Tsuchida et al., 1994); rabbit anti-*Isl1/2*, 1:5,000; rabbit anti-*Lhx3*, 1:5,000 (Sharma et al., 1998); mouse monoclonal anti-En1, 1:100 (Ericson et al., 1997); guinea pig anti-*Chx10*, 1:10,000 (see below); mouse monoclonal 4F2 (anti-*Lhx1/5*), 1:2,000 (Tsuchida et al., 1994); rabbit anti-*Brn3.0*, 1:1,000 (Fedtsova and Turner, 1997); mouse monoclonal anti-*Pax6*, 1:100 (Ericson et al., 1997); mouse monoclonal anti-*Nkx2.2*, 1:100 (Ericson et al., 1997); rabbit anti-HNF-3 β , 1:8,000; rabbit anti-*Lhx2*, 1:8,000; mouse monoclonal immunoglobulin M anti-TAG1, 1:5; mouse monoclonal MPM2, 1:10,000 (Upstate Biotechnology) (Wesendorf et al., 1994); rabbit anti-LacZ, 1:10,000 (Cappel); rat monoclonal anti-BrdU, 1:1,000 (Harlan); and rabbit anti-neurofilament, 1:10,000 (Cappel). Species-specific secondary antibodies conjugated to FITC, Cy3, or aminomethylcoumarin acetate were used as recommended (Jackson Labs). Peroxidase stains were accomplished with ABC (Vector). Images were obtained with a Zeiss Axioptan II microscope and a Princeton Instruments MicroMax cooled charge-coupled device camera and were electronically assigned to red, green, or blue channels. Fluorescence intensity was analyzed with the measurement module of OpenLab 2.0 software (Improvision).

Digoxigenin-labeled riboprobes complementary to *Hb9*, *Isl2*, *Gli1*, *Gli2*, *Gli3*, *Sim1*, and *ChAT* were synthesized according to the suppliers' protocol (Boehringer Mannheim) and used for in situ hybridization as described (Schaeren-Wiemers and Gerfin-Moser, 1993). Diaphorase staining was performed as described (Wetts and Vaughn, 1994).

HB9 Antibodies

A DNA fragment encoding the C-terminal region of mouse HB9 (amino acids 307–403; K. H. et al., submitted) was cloned into pGEX-4T2 (Pharmacia), and fusion protein was purified from *Escherichia coli* with glutathione-sepharose columns. The N-terminal region of HB9 was synthesized as a peptide (amino acids 1–15) and conjugated to haptin. Mouse *Chx10* amino acids 27–143 (Genbank accession number L34808) were expressed as a fusion protein from pGEX-4T1 (Pharmacia) as above.

Whole-Mount Staining

For NMJ visualization, intercostal muscle or diaphragm was dissected from heavily fixed embryos and incubated with rabbit anti-neurofilament, 1:400 (Cappel), and Texas Red-conjugated α -bungarotoxin (α -BTX), 1:750 (Molecular Probes), overnight at 4°C. Whole-mount neurofilament, X-gal staining, and RNA in situ localization were performed as described previously (Harland, 1991; Hogan et al., 1994; Ciu et al., 1997).

Neuronal Fills

Backlabeling of specific MN and interneuron subtypes was performed with 3,000 molecular mass rhodamine-dextran (Molecular Probes). Embryos were cultured in oxygenated mouse Ringer solution for 6–10 hr at room temperature to permit retrograde transport of the label and then fixed for immunocytochemistry. Retrograde and orthograde labeling were performed by injection of Dil in ethanol as described (Sharma et al., 1994). Following injection, embryos were incubated in 4% paraformaldehyde for 1 week at 37°C to permit diffusion. Dil fluorescence was directly photographed or photoconverted to a diaminobenzidine precipitate (Sandell and Masland, 1988).

Mice

Hb9 KO

A mouse lacking functional *Hb9* was generated as described (K. H. et al., submitted). Briefly, a targeting construct containing a "floxed" *neomycin* resistance gene (*neo*) in place of exon 3 (encoding ten amino acids of the homeodomain and the entire C-terminal region of the protein) was used for homologous recombination in mouse embryonic stem cells. After removal of the *neo* cassette with Cre recombinase, identified recombinants were injected into 3.5 day C57BL/6 blastocysts to generate chimeric mice.

Hb9lacZ;wt and Hb9lacZ;KO

A 9 kb NotI fragment of *Hb9* upstream promoter sequence was isolated from a mouse 129sv genomic library (Stratagene) and linked to a nuclear-localized *lacZ* cassette containing a floxed *neo* resistance gene. This construct was targeted by homologous recombination into the 3'-untranslated region of *Isl2* at an SphI site 50 nt downstream of the translational stop codon. This genomic location was chosen to obtain single copy transgenics in a characterized locus. The *neo* cassette was deleted by mating animals to a protamine:Cre line (O'Gorman et al., 1997) to generate *Hb9lacZ;wt* mice. Intercrosses between the progeny of *Hb9* KO and *Hb9lacZ;wt* mice were used to generate *Hb9lacZ;KO* embryos.

Acknowledgments

We thank J. Sheridan, M. McLean, and A. Pope for help with immunocytochemistry. We are indebted to J. Vaughan and J. Rivier for synthesis of the HB9 peptide, S. O'Gorman for Cre mice, W. C. Lin for help with NMJ staining, and T. Jessell for ongoing discussion and immunological reagents. We are grateful to Drs. Funahashi, Jurata, Kintner, Lemke, McKiernan, O'Gorman, and Thomas and to L. O'Brien and A. Leonard for comments on the manuscript. The initial characterization of *Hb9* genomic sequences occurred while S. L. P. was a postdoctoral fellow with T. M. Jessell. The Markey Foundation and the National Institutes of Health provided Medical Scientist Training support for J. T. The Human Frontiers Science Program provided postdoctoral support for K. S. This research was funded by the Whitehall Foundation, the American Paralysis Association, and the National Institutes of Health (grant NS37116). S. L. P. is a Basil O'Connor, McKnight, Pew, and Alfred P. Sloan Scholar.

Received April 29, 1999; revised July 2, 1999.

References

Appel, B., Korzh, V., Glasgow, E., Thor, S., Edlund, T., David, I.B., and Eisen, J.S. (1995). Motoneuron fate specification revealed by patterned LIM homeobox gene expression in embryonic zebrafish. *Development* **121**, 4117-4125.

Arber, S., Han, B., Mendelsohn, M., Smith, M., Jessell, T.M., and Sockanathan, S. (1999). Requirement for the homeobox gene *Hb9* in the consolidation of motor neuron identity. *Neuron* **23**, this issue, 659-674.

Arendt, D., and Nubler-Jung, K. (1999). Comparison of early nerve cord development in insects and vertebrates. *Development* **126**, 2309-2325.

Briscoe, J., Sussel, L., Serup, P., Hartigan-O'Connor, D., Jessell, T.M., Rubenstein, J.L.R., and Ericson, J. (1999). Homeobox gene *Nkx2.2* and specification of neuronal identity by graded sonic hedgehog signaling. *Nature* **398**, 622-627.

Brown, A.G. (1981). Organization in the Spinal Cord: Anatomy and Physiology of Identified Neurons. (Berlin: Springer-Verlag).

Chiang, C., Litingtung, Y., Lee, E., Young, K.E., Corden, J.L., Westphal, H., and Beachy, P.A. (1996). Cyclopia and defective axial patterning in mice lacking Sonic hedgehog gene function. *Nature* **383**, 407-413.

Duboule, D., and Wilkins, A.S. (1998). The evolution of 'bricolage'. *Trends Genet.* **14**, 54-59.

Eizinger, A., Jungblut, B., and Sommer, R.J. (1999). Evolutionary change in the functional specificity of genes. *Trends Genet.* **15**, 197-202.

Ericson, J., Rashbass, P., Schedl, A., Brenner-Morton, S., Kawakami, A., van Heyningen, V., Jessell, T.M., and Briscoe, J. (1997). Pax6 controls progenitor cell identity and neuronal fate in response to graded Shh signaling. *Cell* **90**, 169-180.

Fedtsova, N., and Turner, E.E. (1997). Inhibitory effects of ventral signals on the development of Brn-3.0-expressing neurons in the dorsal spinal cord. *Dev. Biol.* **190**, 18-31.

Greer, J.J., Allan, D.W., Martin-Caraballo, M., and Lemke, R.P. (1999). An overview of phrenic nerve and diaphragm muscle development in the perinatal rat. *J. Appl. Physiol.* **86**, 779-786.

Halpern, M.E., Ho, R.K., Walker, C., and Kimmel, C.B. (1993). Induction of muscle pioneers and floor plate is distinguished by the zebrafish *no tail* mutation. *Cell* **75**, 99-111.

Halpern, M.E., Thisse, C., Ho, R.K., Thisse, B., Riggleman, B., Trevarrow, B., Weinberg, E.S., Postlethwait, J.H., and Kimmel, C.B. (1995). Cell-autonomous shift from axial to paraxial mesodermal development in zebrafish floating head mutants. *Development* **121**, 4257-4264.

Hanna-Rose, W., and Hansen, U. (1996). Active repression mechanisms of eukaryotic transcription repressors. *Trends Genet.* **12**, 229-234.

Harland, R.M. (1991). In situ hybridization: an improved whole-mount method for *Xenopus* embryos. *Methods Cell Biol.* **36**, 685-695.

Harrison, K.A., Druey, K.M., Deguchi, Y., Tuscano, J.M., and Kehrl, J.H. (1994). A novel human homeobox gene distantly related to *proboscipedia* is expressed in lymphoid and pancreatic tissues. *J. Biol. Chem.* **269**, 19968-19975.

Hemavathy, K., Meng, X., and Ip, Y.T. (1997). Differential regulation of gastrulation and neuroectodermal gene expression by Snail in the *Drosophila* embryo. *Development* **124**, 3683-3691.

Hobert, O., and Westphal, H. (1999). Function of LIM homeobox genes. *Trends Genet.*, in press.

Hogan, B., Beddington, R., Costantini, F., and Lacy, E. (1994). Manipulating the Mouse Embryo, Second Edition (Cold Spring Harbor, NY: Cold Spring Harbor Laboratory Press).

Hui, C.C., Slusarski, D., Platt, K.A., Holmgren, R., and Joyner, A.L. (1994). Expression of three mouse homologs of the *Drosophila* segment polarity gene *cubitus interruptus*, *Gli*, *Gli-2*, and *Gli-3*, in ectoderm- and mesoderm-derived tissues suggests multiple roles during postimplantation development. *Dev. Biol.* **162**, 402-413.

Jurata, L.W., Pfaff, S.L., and Gill, G.N. (1998). The nuclear LIM domain interactor NLI mediates homo- and heterodimerization of LIM domain transcription factors. *J. Biol. Chem.* **273**, 3152-3157.

Leber, S.M., Breedlove, S.M., and Sanes, J.R. (1990). Lineage, arrangement, and death of clonally related motoneurons in chick spinal cord. *J. Neurosci.* **10**, 2451-2462.

Lee, K.J., Mendelsohn, M., and Jessell, T.M. (1998). Neuronal patterning by BMPs: a requirement for GDF7 in the generation of a discrete class of commissural interneurons in the mouse spinal cord. *Genes Dev.* **12**, 3394-3407.

Maatman, R., Zachgo, J., and Gossler, A. (1997). The *Danforth's short tail* mutation acts cell autonomously in notochord cells and ventral hindgut endoderm. *Development* **124**, 4019-4028.

Nornes, H.O., and Carry, M. (1978). Neurogenesis in spinal cord of mouse: an autoradiographic analysis. *Brain Res.* **159**, 1-6.

O'Gorman, S., Dagenais, N.A., Qian, M., and Marchuk, Y. (1997). Protamine-Cre recombinase transgenes efficiently recombine target sequences in the male germ line of mice, but not in embryonic stem cells. *Proc. Natl. Acad. Sci. USA* **94**, 14602-14607.

Osumi, N., Hirota, A., Ohuchi, H., Nakafuku, M., Iimura, T., Kuratani, S., Fujiwara, M., Noji, S., and Eto, K. (1997). Pax-6 is involved in the specification of hindbrain motor neuron subtype. *Development* **125**, 2961-2972.

Pfaff, S., and Kintner, C. (1998). Neuronal diversification: development of motor neuron subtypes. *Curr. Opin. Neurobiol.* **8**, 27-36.

Pfaff, S.L., Mendelsohn, M., Stewart, C.L., Edlund, T., and Jessell, T.M. (1996). Requirement for LIM homeobox gene *Isl1* in motor neuron generation reveals a motor neuron-dependent step in interneuron differentiation. *Cell* **84**, 309-320.

Pflugrad, A., Meir, J.Y., Barnes, T.M., and Miller, D.M., III (1997). The

- Groucho*-like transcription factor UNC-37 functions with the neural specificity gene *unc-4* to govern motor neuron identity in *C. elegans*. *Development* 124, 1699–1709.
- Qiu, Y., Pereira, F.A., DeMayo, F.J., Lydon, J.P., Tsai, S.Y., and Tsai, M.J. (1997). Null mutation of mCOUP-TF1 results in defects in morphogenesis of the glossopharyngeal ganglion, axonal projection, and arborization. *Genes Dev.* 11, 1925–1937.
- Rivera-Pomar, R., and Jackle, H. (1996). From gradients to stripes in *Drosophila* embryogenesis: filling in the gaps. *Trends Genet.* 12, 478–483.
- Ross, A.J., Ruiz-Perez, V., Wang, Y., Hagan, D.M., Scherer, S., Lynch, S.A., Lindsay, S., Custard, E., Belloni, E., Wilson, D.I. et al. (1998). A homeobox gene, *HLXB9*, is the major locus for dominantly inherited sacral agenesis. *Nat. Genet.* 20, 358–361.
- Rubenstein, J.L., and Beachy, P.A. (1998). Patterning of the embryonic forebrain. *Curr. Opin. Neurobiol.* 8, 18–26.
- Ruiz i Altaba, A. (1998). Combinatorial *Gli* gene function in floor plate and neuronal inductions by Sonic hedgehog. *Development* 125, 2203–2212.
- Saha, M.S., Miles, R.R., and Grainger, R.M. (1997). Dorsal–ventral patterning during neural induction in *Xenopus*: assessment of spinal cord regionalization with xHB9, a marker for the motor neuron region. *Dev. Biol.* 187, 209–223.
- Sandell, J.H., and Masland, R.H. (1988). Photoconversion of some fluorescent markers to a diaminobenzidine product. *J. Histochem. Cytochem.* 36, 555–559.
- Schaeren-Wiemers, N., and Gerfin-Moser, A. (1993). A single protocol to detect transcripts of various types and expression levels in neural tissue and cultured cells: in situ hybridization using digoxigenin-labeled cRNA probes. *Histochemistry* 100, 431–440.
- Serafini, T., Colamarino, S.A., Leonardo, E.D., Wang, H., Beddington, R., Skarnes, W.C., and Tessier-Lavigne, M. (1996). Netrin-1 is required for commissural axon guidance in the developing vertebrate nervous system. *Cell* 87, 1001–1014.
- Sharma, K., Korade, Z., and Frank, E. (1994). Development of specific muscle and cutaneous sensory projections in cultured segments of spinal cord. *Development* 120, 1315–1323.
- Sharma, K., Sheng, H.Z., Lettieri, K., Li, H., Karavanov, A., Potter, S., Westphal, H., and Pfaff, S.L. (1998). LIM homeobox factors Lhx3 and Lhx4 assign subtype identities for motor neurons. *Cell* 95, 817–828.
- Siegler, M.V., and Jia, X.X. (1999). Engrailed negatively regulates the expression of cell adhesion molecules *Connectin* and *neuroglian* in embryonic *Drosophila* nervous system. *Neuron* 22, 265–276.
- Talbot, W.S., Trevarrow, B., Halpern, M.E., Melby, A.E., Farr, G., Postlethwait, J.H., Jowett, T., Kimmel, C.B., and Kimmel, D. (1995). A homeobox gene essential for zebrafish notochord development. *Nature* 378, 150–157.
- Tanabe, Y., and Jessell, T.M. (1996). Diversity and pattern in the developing spinal cord. *Science* 274, 1115–1122.
- Tanabe, Y., William, C., and Jessell, T.M. (1998). Specification of motor neuron identity by the MNR2 homeobox protein. *Cell* 95, 67–80.
- Thor, S., Andersson, S.G., Tomlinson, A., and Thomas, J.B. (1999). A LIM-homeobox combinatorial code for motor-neuron pathway selection. *Nature* 397, 76–80.
- Tiret, L., Le Mouellic, H., Maury, M., and Brulet, P. (1998). Increased apoptosis of motoneurons and altered somatotopic maps in the brachial spinal cord of Hoxc-8-deficient mice. *Development* 125, 279–291.
- Tsuchida, T., Ensini, M., Morton, S.B., Baldassare, M., Edlund, T., Jessell, T.M., and Pfaff, S.L. (1994). Topographic organization of embryonic motor neurons defined by expression of LIM homeobox genes. *Cell* 79, 957–970.
- Varela-Echavarría, A., Pfaff, S.L., and Guthrie, S. (1996). Differential expression of LIM homeobox genes among motor neuron subpopulations in the developing chick brain stem. *Mol. Cell. Neurosci.* 8, 242–257.
- Westendorf, J.M., Rao, P.N., and Gerace, L. (1994). Cloning of cDNAs for M-phase phosphoproteins recognized by the MPM2 monoclonal antibody and determination of the phosphorylated epitope. *Proc. Natl. Acad. Sci. USA* 91, 714–718.
- Wetts, R., and Vaughn, J.E. (1994). Choline acetyltransferase and NADPH diaphorase are co-expressed in rat spinal cord neurons. *Neuroscience* 63, 1117–1124.
- Xiong, W.C., and Montell, C. (1993). *tramtrack* is a transcriptional repressor required for cell fate determination in the *Drosophila* eye. *Genes Dev.* 7, 1085–1096.

Note Added in Proof

The data referred to throughout as “K.H. et al., submitted” are now in press: Harrison, K.A., Thaler, J., Pfaff, S.L., Gu, H., and Kehrl, J.H. (1999). Pancreas dorsal lobe agenesis and abnormal islets of Langerhans in mice deficient in homeobox factor HB9. *Nat. Genet.*, in press.